THE NONLINEAR DYNAMICS OF TEARING DRIVEN BY STATIC AND ROTATING EXTERNAL 3D FIELDS

S. Inoue
National Institutes for Quantum and Radiological Science and Technology
Naka, Ibaraki 311-0193, Japan
Email: inoue.shizuo@qst.go.jp

M. Okabayashi
Princeton Plasma Physics Laboratory
Princeton, NJ 08543-0451, USA

Z. Taylor
ORAU Oak Ridge Associated Universities
Oak Ridge, TN 37831, USA

E. J. Strait
General Atomics
San Diego, CA 92186-5608, USA

J. Shiraishi, M. Takechi, G. Matsunaga, A. Isayama, N. Hayashi, S. Ide
National Institutes for Quantum and Radiological Science and Technology
Naka, Ibaraki 311-0193, Japan

Abstract

The interaction of a locked tearing mode with a non-axisymmetric control field is numerically explored via nonlinear resistive MHD simulation code "AEOLUS-IT". Locked tearing mode islands often lead to disruptions in tokamaks. Experiments have shown that unlocking and rotating the island using a rotating control field (CF) can postpone or prevent a disruption. The dynamics of this control has been modelled with the AEOLUS-IT code in both tearing stable and unstable plasmas. The fundamental responses of penetration and screening of the CF and static error field have been identified and characterized in both tearing stable and unstable model plasmas. Forced-rotation of the CF prevents the EF penetration in both plasmas, which is characterized with a finite slip frequency between plasmas and the CF. On the other hand, the magnetic island rotating frame is different between tearing stable and unstable plasmas. The magnetic island rotates with the external fields in tearing stable plasmas, while it coalesces with the plasmas. Furthermore, model predictions of two distinct regimes of plasma responses, characterized as standing-wave and traveling-wave responses, are in qualitative agreement with DIII-D observations. These results are an important step toward predictive understanding of this approach to tearing mode control and disruption avoidance.

1. INTRODUCTION

Locked modes, where magnetic islands are locked in the lab frame by electromagnetic torque from induced wall currents and static error fields (EFs) [1], are frequently observed in tokamak experiments and are a main cause of plasma disruptions [2, 3]. Development of disruption avoidance schemes is an urgent issue for ITER and DEMO, and active control schemes for locked modes are indispensable. For locked mode control, both release of the locked magnetic island from the static EF torque and suppression/stabilization of the island are essential. In present devices, external resonant magnetic fields are widely used to control the phase of the magnetic island. Rotating resonant magnetic control fields (CFs) utilized for locked tearing mode control have successfully released locked magnetic islands and recovered the island rotation [4]. Here, the key physics for control of the locked modes is the screening/penetration of external fields, i.e. the EF and the CF. The transition between the screening and the penetration of the external fields depends on the frequency of the CF, amplitudes of both the EF and the CF, and the background equilibrium plasma rotation. These dependencies were recently numerically investigated inside tearing stable plasmas with realistic dissipation parameters using the nonlinear, resistive MHD code "AEOLUS-IT" [5,6]. In this paper, we extend our work with tearing unstable plasmas and a comparison between the tearing stable and unstable plasmas provides an indispensable understanding of dynamics of tearing mode control. We note that even inside the tearing unstable plasmas, tearing stable rational surfaces exist. Thus, understanding the mode locking behaviour inside both the tearing stable and unstable plasma regimes and the interaction between them is essential. The remainder of the paper is organized as follows. First, in section 2, the dependence of the mode locking/unlocking on the CF frequency (ω_{cf}) is numerically investigated in a tearing stable plasma under JT-60SA relevant dissipation parameters, where the Lundquist number (S) is 10^8 and a momentum diffusion time normalized by the poloidal Alfven time ($\tilde{\nu}^{-1} = t_D/t_A$) is 10^5. The safety factor is

assumed such that $q = 1.2(1 + (r/0.6060)^4)^{1/2}$. Here, the tearing stability index is $\Delta' = -4.23$. Next, in section 3, we carried out a simulation in a tearing unstable plasma under DIII-D relevant plasma parameters, such that $S \simeq 0.87 \times 10^7$ and $t_D/t_A \simeq 0.87 \times 10^6$. The safety factor is with analytical form; $q = 1.2(1 + (r/0.62)^{10})^{1/4}$, where $\Delta' = 1.43$. These simulation parameters are summarized in Table 1. The simulation model is the same as in [5, 6]. Lastly, we will present a summary and discussion in section 4.

TABLE 1. Simulation parameters for tearing stable and unstable plasmas.

Simulation run	S	t_D/t_A	Δ'	$\frac{b^r_{21,\mathrm{EF}}}{b_{p0}}$	$\frac{b^r_{21,\mathrm{CF}}}{b_{p0}}$	ω_{CF} [Hz]
1	10^8	10^5	-4.23	5×10^{-5}	2×10^{-4}	20-400
2	0.87×10^7	0.87×10^6	1.43	1×10^{-7}	1×10^{-5}	20-6000
3	0.87×10^7	0.87×10^6	1.43	5×10^{-5}	2.5×10^{-5} $\rightarrow 1 \times 10^{-4}$	75

2. TEARING STABLE CASE (SIMULATION RUN #1)

In tearing stable plasmas, the magnetic island growth is purely driven by external fields, the CF and the EF in our simulation. Thus, the growth and rotation of the magnetic island are strongly coupled with the screening/penetration of the EF and the CF. Figure 1(a) shows the dependence of the island growth rate on the CF rotation frequency (ω_{cf}). A positive growth rate indicates that the external fields (the EF and/or the CF in our simulation) drive forced magnetic reconnection. Figure 1(b) shows the plasma rotational frequency dependence on the CF frequency. The plasma rotational frequency of the (m, n) mode is calculated from the fluid m/n rotation as

$$\omega_{mn} = m v^{\theta}_{00} + n v^{\varphi}_{00},$$

where v^{θ}_{00} and v^{φ}_{00} denote $m/n = 0/0$ component of the poloidal and the toroidal rotation (contravariant component), respectively. In our simulation, there are three characteristic frequencies, such as, the plasma 2/1 rotational frequency (ω_{21}), frequencies of external fields (ω_{CF} and $\omega_{EF} = 0$), and a magnetic island frequency (ω_{is}). For example, when the island remains static in the frame of plasmas, $\omega_{is} = \omega_{21}$. At the low frequency range labelled by (I) in figure 1, the plasma rotational frequency linearly increases with increasing CF frequency, which indicates that the magnetic island rotates with the CF. In this frequency range, the CF penetrates into the rational surface and drives magnetic island growth. The plasma starts to slip from the CF at higher CF frequencies, which can be seen in the sudden end of the linear increase of the plasma rotational frequency in figure 1(b). The difference of the rotational frequency between the external fields and the plasmas brings the shielding effect of the external fields. Here, the plasma rotational frequency still remains finite valued, which can prevent EF penetration. Thus, during the (II) frequency range, both the EF and the CF do not penetrate into the rational surface and the island growth-rate remains zero as shown in the figure 1(a). The slip between the CF and the plasma becomes large at still larger CF frequencies, which results in the deceleration of the plasma rotation. When the remaining plasma rotation is not sufficient to shield out the EF penetration, the EF penetrates into the rational surface, damps the plasma rotation and drives the positive island growth rate shown in the figure 1. However, the plasma rotation is diffusively driven with further increases of the CF frequency. When the diffusively driven plasma rotation is sufficient to shield the EF penetration, the magnetic island growth becomes zero again as shown in figure 1(b).

Figure 2 shows typical spatial profiles of (a) the radial magnetic field, (b) the poloidal plasma rotation, and (c) force balance between electromagnetic (solid), viscous (dashed), and inertia (dash-dotted) torque. The CF frequency of each plot is indicated in figure 1(a). When the CF penetrates into the rational surface, the even parity mode grows and the finite plasma rotation exists around the rational surface. If both external fields (EF and CF) are shielded, the structure of the mode is changed from an even to odd-type parity, which is labeled by 1 (dashed) and 3 (dotted) in figure 2. In these frequency ranges, there are finite plasma rotation at the rational surface but its frequency is different from that of the CF, which indicates that both the EF and the CF are screened out by the plasma. During the locked mode period where the EF penetrates into the rational surface (case 2 with dash-dotted curve), an even parity mode is superimposed over an odd parity mode. The typical poloidal force balance of $m/n = 0/0$ mode for case 0 (penetrated) and case 1 (screened) is shown in figure 2(c). Each torque is calculated by

$$T^{\theta}_{\mathrm{jxB},00} = \sum_{00}(\boldsymbol{j}_{m'n'} \times \boldsymbol{B}_{m''n''} \cdot \nabla\theta),$$

$T^{\theta}_{V,00} = \tilde{\nu}\nabla^2 \boldsymbol{v}_{00} \cdot \nabla\theta,$

$T^{\theta}_{I,00} = \sum_{00}(\boldsymbol{v}_{m'n'} \cdot \nabla \boldsymbol{v}_{m''n''} \cdot \nabla\theta),$

where $\sum_{00}$ calculates mode coupling satisfying $m' + m''$ and $n' + n'' = 0$. The resonant electromagnetic torque is localized around the rational surface, which is mainly balanced with viscous torque.

The temporal behavior of the island is shown in figure 3. Here, the phase difference $\Delta\theta$ indicates the phase difference between the mode and the CF for the cases 0 and 1, and between the mode and the EF for the cases 2 and 3. As shown in the figure 3(a), the temporal evolution of the island phase continuously rotates in the cases 0 and 1. A difference can be seen, however, in the phase between the mode and the CF shown in figure 3(b). Although the island phase continuously rotates in both cases, the phase is shifted 90 degrees from the CF in case 1, which is an anti-phase against the CF. The stabilization effect of the external field is maximized when the mode phase becomes anti-phase against the external field [7]. Thus, in case 1, the island growth is stabilized. In addition, in case 1, the island rotational frequency (ω_{is}) no longer corresponds to the plasma rotational frequency (ω_{21}). The ω_{21} of case 1 is half of that of the case 0 as shown in figure 1(b), while the ω_{is} is approximately the same as seen in cases 0 and 1 in figure 3(a), which indicates that the mode rotates with the CF and the plasma is slipped from both. In cases 2 and 3, the island phase no longer rotates but is fluctuating as shown in figure 3(a). We note that these two modes can be seen as the standing-wave like responses, where the amplitude of the mode is up and down, but the mode itself is standing. Although the temporal behavior is similar between cases 2 and 3, the phase shift from the EF is different between these two cases. The averaged phase difference is 90 degrees (anti-phase) in case 3, while it is ~30 degrees in case 2. The even parity mode is thus completely stabilized in case 3, while it co-exists with the odd-parity mode in case 2.

The dependences of plasma and magnetic island rotational behaviors on the CF frequency are summarized in Table 2. The magnetic island is in-phase with the external fields when the external fields penetrate and is anti-aligned when they are shielded out. During field penetration, the plasma also co-rotates with both the magnetic island and the external fields, while it slips from both when the external field is screened out. An identification of the stable frequency range is required for successful control of the locked mode. Our nonlinear simulation clarifies that (1) rotational frequency differences between the plasma and the island or the external fields, (2) anti-aligned phase between the island against the external fields, and (3) the odd-parity radial magnetic field profile is physical characteristic of the stable frequency range.

TABLE 2. Summaries of dependence of mode behavior on a rotating 3D field frequency in the tearing stable plasmas.

	EF	CF	Plasma (ω_{21})	Island (ω_{is}, θ_{is})
Low ω_{CF} ↓ High ω_{CF}	Screened	Penetrated	ω_{CF}	ω_{CF}, in-phase
	Screened	Screened	ω_{Slip}	ω_{CF}, anti-phase
	Penetrated	Screened	ω_{EF}	ω_{EF}, in-phase
	Screened	Screened	ω_{Slip}	ω_{EF}, anti-phase

3. TEARING UNSTABLE CASE (SIMULATION RUN #2)

In our simulation of tearing unstable plasmas, the external field turns on after saturation of the tearing mode growth, which is a relevant condition with the locked mode entrainment experiment [4]. Due to the presence of the nonlinearly-saturated magnetic island, which reaches 18% of minor radius, the CF hardly slips from the plasma over a wide range of frequencies. When the CF is finally rotated fast enough to slip, the magnetic island easily locks to the static EF. Therefore, to obtain the frequency ranges (II) and (III) in figure 1, there are two necessary conditions. First, a very small amplitude of the CF is required for slipping of the CF within a realistically low frequency range, which is in the range of Hz - kHz. Second, very small EF amplitude in comparison with the CF amplitude is required. The results shown here use the simulation parameters of run 2 in Table 1. We note that the EF and the CF in the real experiment are several orders of magnitude higher than those of our simulation. Thus, we set these simulation parameters from the physics point of view. Figure 4 shows the dependence of the island growth rate on the CF frequency (ω_{cf}). The growth rate indicates whether the external fields have a stabilizing effect on the nonlinearly saturated magnetic island. In the low frequency range, the plasma rotation linearly increases with the CF. The CF penetrates into the rational surface and the forced magnetic reconnection of the CF over-drives the magnetic island growth. At higher CF frequencies, the plasma starts to slip from the CF.

Figure 5(a) shows the spatial profile of the radial magnetic field for multiple CF frequencies. The island separatrices are shown by black dashed-lines. Since the intrinsic saturated tearing mode is dominant in our simulation condition, the variation of each case is negligible. In the previous tearing stable plasmas, the rotational profile was sharply peaked around the rational surface. Although the flow-shear around the separatrix of case 0 (solid line) is stronger than that of the case 1 (dashed line), the island growth rate is negative in case 1 while it is positive in case 0, which indicates that the flow-shear has little stabilization effect and the phase shift between the plasma and the CF determines the suppression of the magnetic island. Figure 5(c) shows temporal evolution of volume-averaged torque inside the magnetic island. Here again, the electromagnetic torque is balanced by the viscous torque and the inertia torque is negligible. Figure 6 shows the temporal evolution of the magnetic island phase. The phase evolution from the plasma 2/1 rotation (ω_{21}) is also shown by the triangles. Therefore, the magnetic island always moves with the plasma 2/1 rotation, which is a major difference from the tearing stable plasmas, where the island rotates with external fields and is slipped from plasma when the EF and the CF are screened out. The CF frequencies of the plotted 4 cases are indicated in figure 4. First, in case 0, the mode frequency corresponds to the CF frequency. In this case, the CF penetrates into the rational surface and the island growth rate is positive as shown in figure 4. Second, in cases 1 and 2, the rotational frequency of the mode is suddenly decelerated and exhibits a sharp decay, as shown in figure 6. Here, the island slowly rotates with the plasma, and the CF is slipped from both. Lastly, in case 3, the rotation of both the island and the plasma is damping, which indicates the island locking to the EF.

The dependences of plasma and magnetic island rotational behaviors on the CF frequency are summarized in Table 3. Although the screening/penetration of the EF and the CF are similar to the tearing stable plasmas, the magnetic island co-rotates with the plasma (not the CF) in the partial penetration states. Thus, the external field is slipped both from the plasma and the magnetic island when the external field is screened out, and the plasma is strongly coupled with the magnetic island due to the strong electromagnetic torque brought by the magnetic island.

TABLE 3. Summaries of dependence of mode behavior on a rotating 3D field frequency in the tearing unstable plasmas.

	EF	CF	Plasma (ω_{21})	Island (ω_{is}, θ_{is})
Low ω_{CF} ↓ High ω_{CF}	Screened	Penetrated	ω_{CF}	ω_{CF}, in-phase
	Screened	Screened	ω_{Slip}	ω_{Slip}, slip
	Penetrated	Screened	ω_{EF}	ω_{EF}, finite-shift

4. SUMMARY AND DISCUSSION

The screening/penetration with both the error field (EF) and the rotating control field (CF) inside tearing stable and unstable plasmas have been herein investigated via the nonlinear MHD code "AEOLUS-IT", which focuses on the key physics for tearing mode control via rotating-3D fields. Various types of responses to the rotating CF have been classified in both the tearing stable and unstable plasmas. In tearing stable plasmas, the external field itself drives the mode. Thus, when the external field is screened out by the plasma, the mode moves with the external field with finite phase shift and plasma rotation is different from both. In the tearing unstable plasmas, a non-linearly saturated intrinsic mode is dominant over the externally driven modes. Thus, when the external field is screened out by the plasma, the mode moves with the plasma and the external field is slips away from both. For experimental application of the 3D rotating field for the locked mode avoidance, these dependences of tearing modes locking/unlocking on rotating 3D fields are all important since experimental plasmas often incorporate both tearing stable and unstable rational surfaces that interact each other. Dependences of the mode behavior on the external field amplitude were recently investigated in the DIII-D device, as shown in figure 7. The experimental condition was the ITER baseline scenario with q95=3.2-3.8. The frequency of the external 3D field was 75Hz. In this experiment, the 3D field coil current was increased by 30%, from 3.1 to 4.3 kA in the middle of the discharge. Figure 7(a) shows two magnetic sensors signals at 97 and 200 degrees toroidally. In phase I, where the region is hatched by red and the 3D field coil current is 3.1kA, the sensor signal oscillation amplitude is half that of phase II, where the region is hatched by blue and the 3D field coil current is 4.3kA. Figure 7(b) shows the toroidal angle dependence of the mode and each curve is a regularly spaced time step within one cycle of the 3D field. As shown in the figure, the response of the mode clearly changes from a standing-wave type response in phase I to a travelling-wave type response in phase II. Thus, not only the amplitude but also temporal behavior of the mode is different between these two phases. A corresponding simulation was carried out by AEOLUS-IT, where magnetic Lundquist number, safety-factor profile, and the frequency of the rotating-3D field was calculated with DIII-D relevant experimental parameters as shown as run 3 in table 1. The response observed

in the DIII-D experiment was reproduced in our reduced cylindrical model by artificially increasing of the rotating field amplitude from 50% to 200% of the EF amplitude. We note that the frequency of the rotating field is too slow to be screened out by plasmas as shown in figure 4, where the required CF frequency for the screening is several kHz. We note that the amplitude of the CF in run 2 is 10% of that in run 3, which indicates that the required frequency for the screening in run 3 would be higher than that in run 2. Although the required CF frequency for screening of the intrinsic 2/1 mode is extremely high in comparison with the wall resistive frequency, ~200Hz [8], the externally driven modes, such as m/n=3/2, 3/1, and 4/1 modes, can be screened with relatively lower frequency as shown in figure 1, where the CF is screened out with 50Hz. In the real experiment, the 3D rotating field incorporates multiple poloidal and toroidal modes. The non-linear screening/penetration of the externally driven modes can also be coupled with the intrinsic 2/1 mode through the toroidicity. More detailed experimental explorations will be presented by another paper [9].

In conclusion, our non-linear simulation has characterized detailed mode locking/unlocking behavior with single-helicity assumption. However, a multi-helicity interaction that incorporates both tearing stable/unstable rational surfaces and externally/internally driven modes will be needed for robust avoidance of the locked tearing mode via rotating fields since multi-helicity interactions can be important in experimental devices [9]. Future AUOLUS-IT modelling including multiple helicities will build on this work and characterize coupled multi-mode dynamics.

ACKNOWLEDGEMENTS

This work was supported by JSPS KAKENHI Grant Numbers 17K07003.

This material is based upon work supported by the U.S. Department of Energy, Office of Science, Office of Fusion Energy Sciences, using the DIII-D National Fusion Facility, a DOE Office of Science user facility, under Awards DE-FC02-04ER54698. DIII-D data shown in this paper can be obtained in digital format by following the links at https://fusion.gat.com/global/D3D_DMP. **Disclaimer:** This report was prepared as an account of work sponsored by an agency of the United States Government. Neither the United States Government nor any agency thereof, nor any of their employees, makes any warranty, express or implied, or assumes any legal liability or responsibility for the accuracy, completeness, or usefulness of any information, apparatus, product, or process disclosed, or represents that its use would not infringe privately owned rights. Reference herein to any specific commercial product, process, or service by trade name, trademark, manufacturer, or otherwise does not necessarily constitute or imply its endorsement, recommendation, or favoring by the United States Government or any agency thereof. The views and opinions of authors expressed herein do not necessarily state or reflect those of the United States Government or any agency thereof.

REFERENCES

[1] Nave M F F and Wesson J A 1990 Nuclear Fusion 30 2575–2583.

[2] de Vries P C, Johnson M F, Alper B, Buratti P, Hender T C, Koslowski H R, Riccardo V and JET-EFDA contributors 2011 Nuclear Fusion 51 053018.

[3] Sweeney R, Choi W, La Haye R J, Mao S, Olofsson K E J, Volpe F A and the DIII-D Team 2016 Nuclear Fusion 57 016019–22.

[4] Okabayashi M, Zanca P, Strait E J, Garofalo A M, Hanson J M, In Y, La Haye R J, Marrelli L, Martin P, Paccagnella R, Paz-Soldan C, Piovesan P, Piron C, Piron L, Shiraki D, Volpe F A and The DIII-D and RFX-mod Teams 2017 Nuclear Fusion 1–13.

[5] Inoue S, Shiraishi J, Takechi M, Matsunaga G, Isayama A, Hayashi N and Ide S 2017 Nuclear Fusion 57 116020–11.

[6] Inoue S, Shiraishi J, Takechi M, Matsunaga G, Isayama A, Hayashi N and Ide S 2017 Plasma Physics and Controlled Fusion 60 025003–10.

[7] Fitzpatrick R 1993 Nuclear Fusion 33 1049–1084.

[8] Logan NC, Strait EJ, Reimerdes H, 2017 Plasma Physics and Controlled Fusion 52 045013.

[9] Okabayashi M, Inoue S, Strait E, Taylor Z, Paz-Soldan C, Ferraro N, Hanson J, Jardin S, La Haye R J, Logan N, in this conference, EX/P6-25.

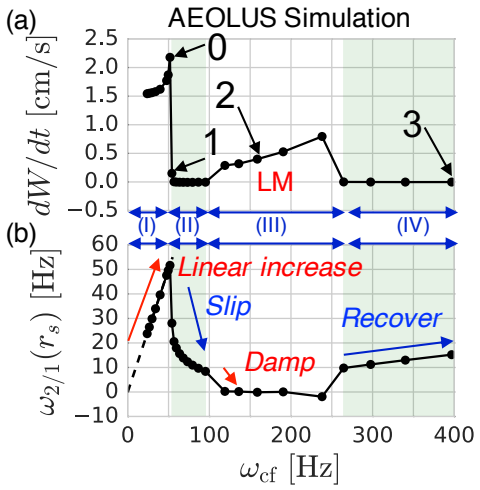

Fig. 1: (a) Dependence of the island growth rate on the CF frequency (ω_{cf}). The positive growth rate indicates that the external fields, which is brought by both the EF and the CF, drives forced magnetic reconnection. (b) Dependence of the 2/1 mode rotational frequency on the CF frequency.

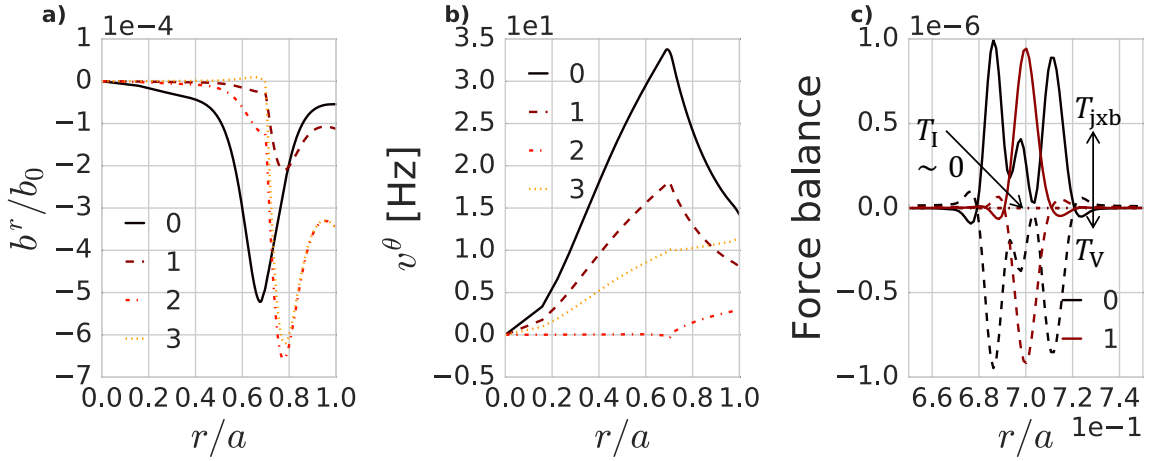

Fig. 2: Spatial profile of (a) the radial magnetic field, (b) the poloidal plasma rotation, and (c) force balance between Lorentz (solid), viscous (dashed), and inertia (dash-dotted) torque. The CF frequency of each slice is indicated in figure 1(a).

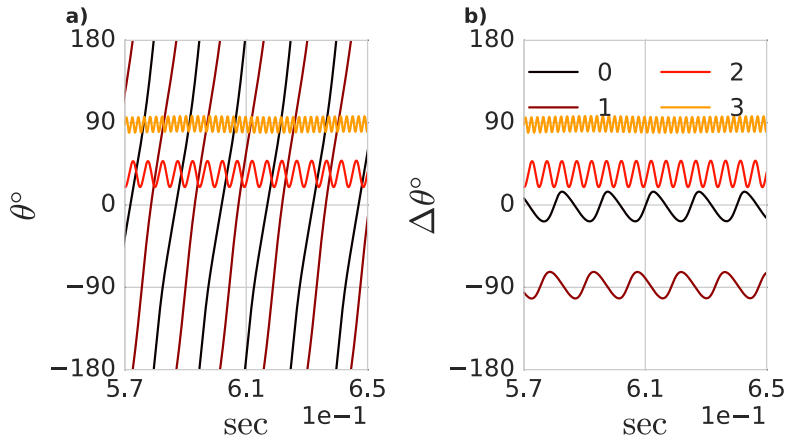

Fig. 3: Temporal evolution of (a) the mode phase and (b) its shift from the CF (cases 0 and 1) and the EF (cases 2 and 3).

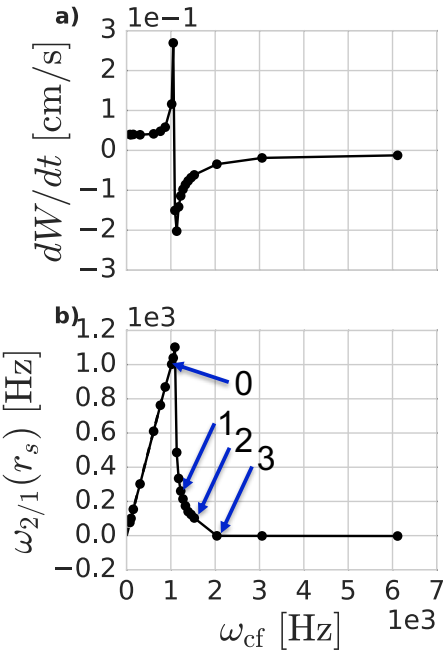

Fig. 4: (a) Dependence of (a) the island growth rate and (b) the 2/1 mode rotational frequency on the CF

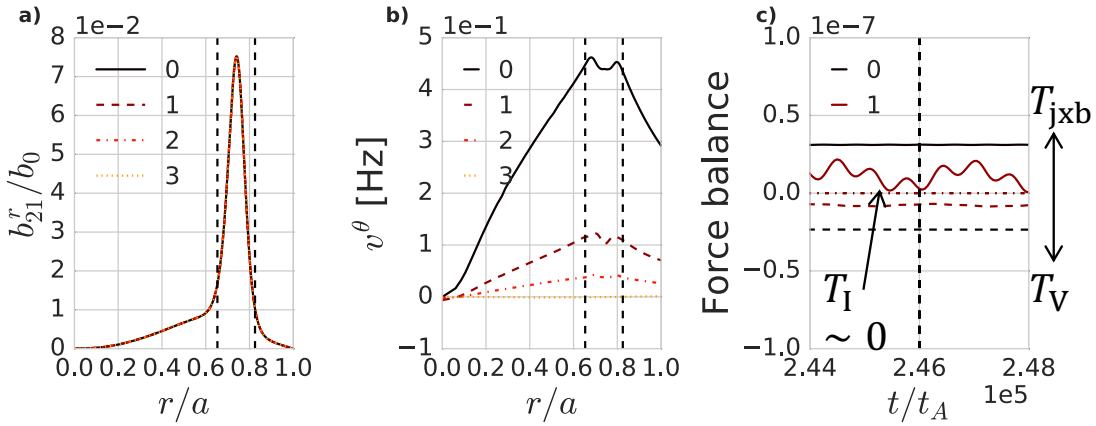

Fig. 5: Spatial profile of (a) the normal component of the magnetic field and (b) the poloidal plasma rotation. (c) Temporal evolution of volume integrated torque inside the magnetic island. The Lorentz, viscous, and inertia torque are shown by solid, dashed, and dash-dotted line. The time for the profile in figure (a) and (b) is indicated by the vertical black dashed line. The CF frequency of each slice is indicated in figure 4(a).

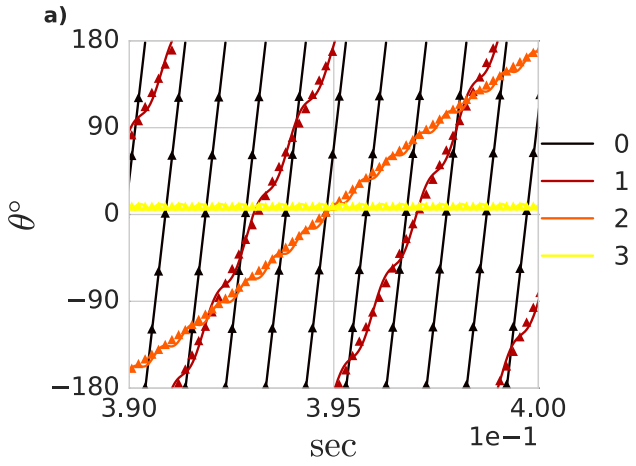

Fig. 6: Temporal evolution of the magnetic island phase. Triangle markers indicate the phase evolution from the plasma 2/1 rotation (ω_{21}).

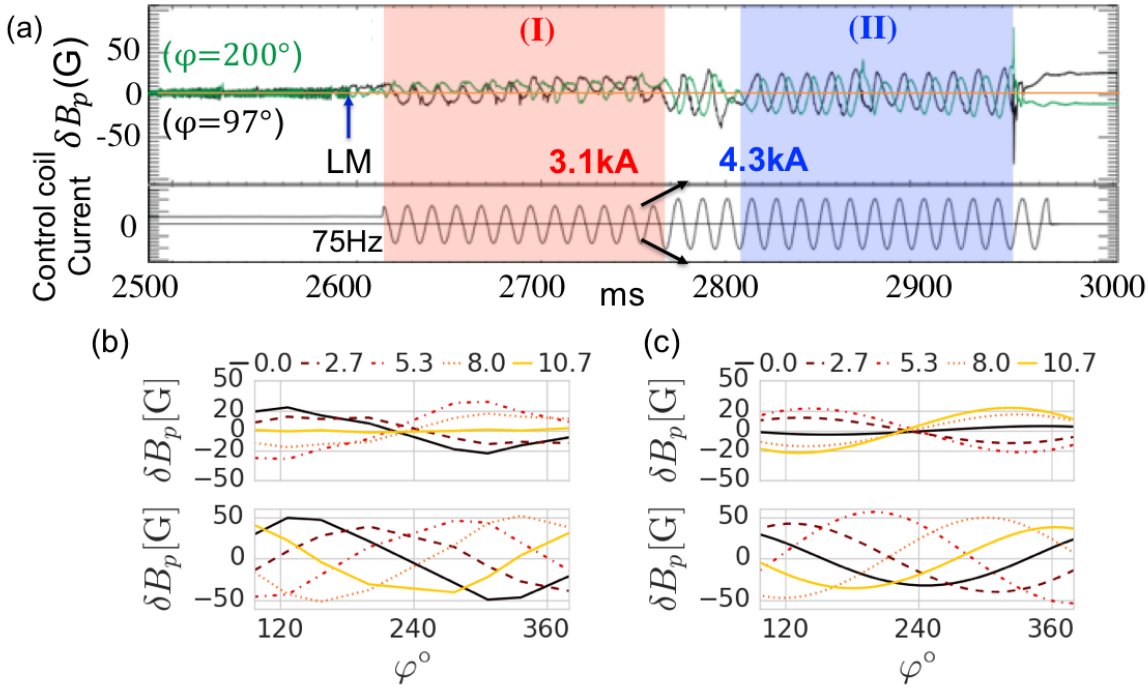

Fig. 7: (a) Temporal evolution of magnetic sensor signals at two different toroidal angles ($\varphi = 97^{\circ}$ and 200°) and rotating I-coil current. Temporal evolution of toroidal angle dependence of the poloidal magnetic field at the plasma surface in the case with (a) AEOLUS simulation and (b) DIII-D #170569. Time evolves from the heavy (black) to the light (yellow) colors of lines.